Available online at www.sciencedirect.com
SCIENCE DIRECT®
Scripta Materialia 50 (2004) 937–941
Scripta MATERIALIA
www.actamat-journals.com

Textures in cold-rolled and annealed $Ti_{50}Ni_{50}$ shape memory alloy

S.H. Chang, S.K. Wu *

Department of Materials Science and Engineering, National Taiwan University, 1, Roosevelt Road, Sec. 4, Taipei 106, Taiwan

Received 26 August 2003; received in revised form 16 December 2003; accepted 13 January 2004

Abstract

In the 50% cold-rolled and 600 °C annealed $Ti_{50}Ni_{50}$ alloy, this study observes $(1\,1\,0)[1\,\bar{1}\,0]_P$ α-fiber II in RD as the main texture in the B2 phase by ODF test. Cyclic tensile tests and DMA results indicate that $(1\,1\,\bar{1})[1\,\bar{1}\,1]_M$ is the main texture in B19′ martensite.

Keywords: Shape memory alloy; Cold-rolling and annealing; Texture; Tension test; Dynamic mechanical analysis

1. Introduction

Near-equiatomic TiNi alloys are important shape memory alloys (SMAs) with good shape memory effect (SME), superelasticity (PE) and damping capacity (DC) [1]. It is well known that the SME of the TiNi single crystal is dependent on its crystal orientation, and that of TiNi polycrystalline SMAs is affected by the texture. Eucken and Hirsch [2] reported that the hot-rolled sheet with $\{1\,1\,0\}\langle 1\,\bar{1}\,0\rangle_P$ texture had its highest tensile shape memory strain in the rolling direction. Here, the subscript p indicates the TiNi parent B2 (CsCl) phase. Lin et al. [3] described the microstructure changes of TiNi martensite with cold-rolling and showed that the stress exerted by cold-rolling caused the martensite variants to coalesce and the internal twinning interfaces to move.

Mulder et al. [4] calculated the theoretical orientation dependence of the transformation strain by considering correspondence variants in $\{1\,1\,0\}\langle 1\,\bar{1}\,0\rangle_P$ texture and comparing it with the observed experimental results. Inoue et al. [5] reported the quantitative texture analysis of the exact texture in the polycrystalline TiNi SMA by orientation distribution function (ODF), and compared the theoretical planar anisotropies of the shape memory strain with the experimental results. Shu and Bhattacharya [6] developed a model to show that the texture is a crucial factor in determining the SME in SMAs' polycrystals, and thus the texture control can be used to improve the SME of SMAs. Miyazaki et al. [7] reported that the transformation strain depended on direction on the specimen plane of the TiNi rolled thin plane, while it was almost the same irrespective of direction in the sputter-deposited TiNi thin films.

In the present work, the textures of different depths of cold-rolled $Ti_{50}Ni_{50}$ sheets were determined first by ODF calculation in the B2 parent phase. Then the anisotropies of mechanical properties corresponding to the texture distribution in these sheets were measured by cyclic tensile tests and dynamic mechanical analysis (DMA). Finally the relationship between the textures and the anisotropies of mechanical properties was established and discussed.

2. Experimental

The $Ti_{50}Ni_{50}$ alloy was prepared by the conventional vacuum arc remelting technique. The as-melted ingot was heated to 900 °C for hot-rolling into a 2 mm thickness plate, and then cold-rolled into 1 mm thickness plate in order to reach 50% cold-rolling reduction. Transformation temperatures of the specimens were determined by differential scanning calorimetry (DSC) with TA Q10 equipment at heating and cooling rates of 10 °C/min.

Specimens for ODF measurements were polished mechanically and then electrically to reduce their thicknesses to three-fourth or half of the original plate thickness. Surface textures, 3/4- and 1/2-thickness of the specimens were calculated from the X-ray pole figure

* Corresponding author. Tel.: +886-223-637-846; fax: +886-223-634-562.
E-mail address: skw@ccms.ntu.edu.tw (S.K. Wu).

1359-6462/$ - see front matter
doi:10.1016/j.scriptamat.2004.01.009

measurements. The pole figures were measured by Siemens D500 diffractometer with back-reflection technique and Mo-radiation. The ODF, including odd terms and ghost correction, was calculated up to an order of $l_{max} = 22$ by the series expansion method [8].

Specimens for cyclic tensile tests were cut in directions $\theta = 0°$, 30°, 60°, 90° to rolling direction (RD). Here, $\theta = 90°$ is the transverse direction (TD). The cyclic tensile tests were carried out at 80 °C with the strain rate of 0.6 mm/min. Each specimen was loaded and set to a constant strain of 4%, and then unloaded to 0 MPa for each cycle N during the cyclic tensile tests. All specimens of four different θ directions were tested for 24 cycles.

Specimens for DMA experiments were cut in the directions $\theta = 0°$, 30°, 60°, 90° to RD. Tan delta and storage modulus of each specimen were measured by TA 2980 DMA equipment with heating and cooling rates of 3 °C/min. The amplitude used on the specimen was 2 μm with the frequency of 2 Hz.

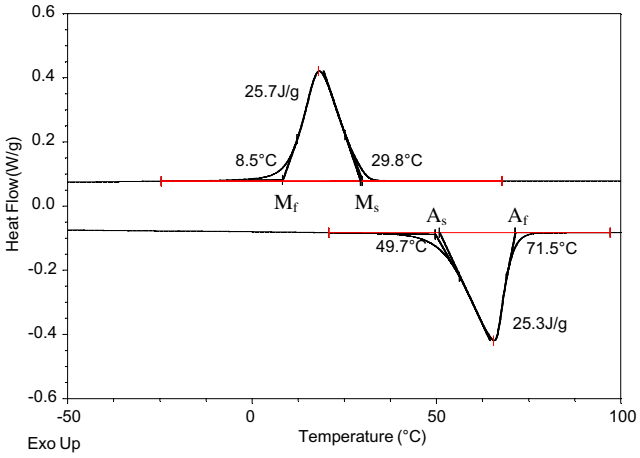

Fig. 1. DSC cooling–heating curve for 50% cold-rolling reduction and annealed at 600 °C for 1 h of the $Ti_{50}Ni_{50}$ sheet.

3. Results and discussion

3.1. DSC and ODF measurements

Transformation temperatures of the specimen 50% cold-rolled and annealed at 600 °C for 1 h are $M_s = 29.8$ °C, $M_f = 8.5$ °C, $A_s = 49.7$ °C, and $A_f = 71.5$ °C, as shown in Fig. 1. Here, M_s and M_f are start and finish temperature of forward martensitic transformation, respectively. A_s and A_f are those of reversed martensitic transformation, respectively. The cyclic tensile tests of Section 3.2 were conducted at 80 °C which is higher than A_f temperature, therefore, the PE property of TiNi B2 parent phase can be measured by cyclic tensile tests.

Fig. 2 shows that $\varphi_2 = 45°$ section of ODFs calculated from a cold-rolled TiNi sheet in different depths of the specimen. The $\varphi_2 = 45°$ section of ODF is used for comparing textures since most of the preferred orientations are conveniently observed in this section. Fig. 2(a) illustrates the ODF calculated from the specimen surface in B2 parent phase. From Fig. 2(a), the texture consists of two components, $(3\,3\,1)[1\,\bar{1}\,0]_P$ in RD and $(1\,1\,1)[1\,\bar{1}\,0]_P$ γ-fiber in normal direction (ND). The orientation densities of these two fibers are almost the same, but $(3\,3\,1)[1\,\bar{1}\,0]_P$ is sharper and $(1\,1\,1)[1\,\bar{1}\,0]_P$ γ-fiber is spread further from the line of $\Phi = 55°$, resembling $\{1\,1\,1\}\langle uvw\rangle_P$ fiber texture along ND in B2

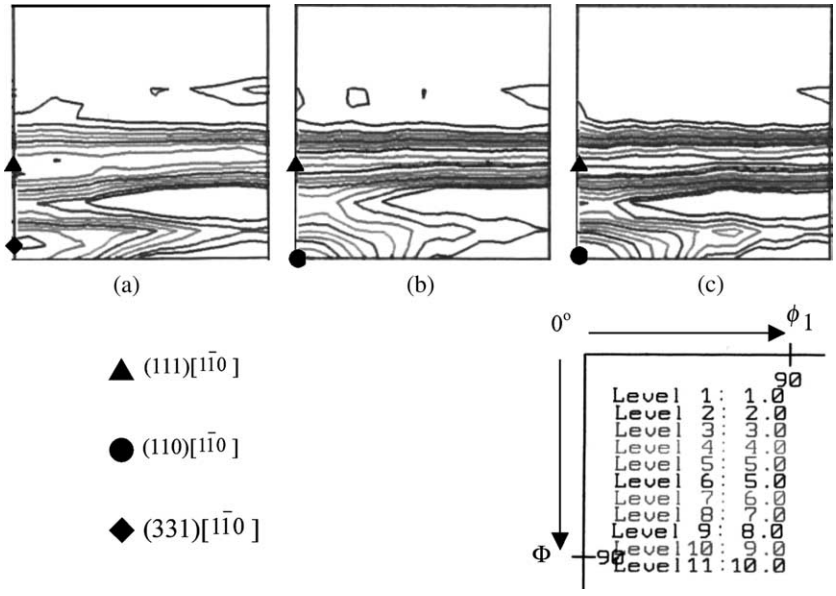

Fig. 2. $\varphi_2 = 45°$ section of orientation distribution functions calculated from various depths of the cold-rolled TiNi sheet: (a) specimen surface, (b) 3/4 thickness of the specimens and (c) 1/2 thickness of the specimens.

structure [5]. Fig. 2(b) shows the ODF calculated from the textures at 3/4 specimen thickness. From this ODF result, the $(3\,3\,1)[1\,\bar{1}\,0]_P$ fiber, as observed in Fig. 2(a), shifts to be the $(1\,1\,0)[1\,\bar{1}\,0]_P$ α-fiber II and its relative orientation density is higher than that of $(1\,1\,1)[1\,\bar{1}\,0]_P$ γ-fiber. The $(1\,1\,0)[1\,\bar{1}\,0]_P$ α-fiber II in RD is not common in general, but is observed generally in TiNi SMAs [9]. Fig. 2(c) is the ODF calculated from the textures at 1/2 specimen thickness. The orientation distribution of Fig. 2(c) is similar to the results of Fig. 2(a) and (b), indicating that the textures in different depths of the specimen are almost the same. Among these three ODFs, the α-fiber II has higher orientation density than γ-fiber, and the intensity of γ-fiber decreases from the surface to the 1/2 specimen thickness. This is because the surface texture is more affected by the shearing effect caused by the friction of rollers. This also induces more γ-fibers in ND occurring at the surface, as shown in Fig. 2(a). As a result, the $(1\,1\,0)[1\,\bar{1}\,0]_P$ α-fiber II along RD can be regarded as the main texture appearing in cold-rolled $Ti_{50}Ni_{50}$ SMA.

3.2. Cyclic tensile tests and discussion

Fig. 3 shows the stress–strain curves obtained from the cyclic tensile tests of the specimens loaded in the directions of $\theta = 0°$, 30°, 60°, 90° to RD from $N = 1$ to 24. After 24 cycles, all specimens can reach good linear superelastic behavior, although they have different permanent strain and loaded stress, as shown in Fig. 3.

From Fig. 3, the specimen of TD ($\theta = 90°$) has the largest loaded stress, about 680 MPa, than the other specimens' directions. This is because TD has the smallest stress-induced-martensite (SIM) strain in all directions [4], and needs the largest stress in this direction if the same 4% strain is to be reached.

From Fig. 3, the measured permanent strains of the four specimens after 24 cycles are listed in Table 1. From Table 1, the specimen of $\theta = 30°$ to RD has the largest permanent strain of 5.8%, and those of $\theta = 0°$ (RD) and $\theta = 60°$ are 4.9% and 3.8%, respectively. TD ($\theta = 90°$) has the smallest permanent strain, of only 2.7%. The experimentally observed permanent strains may be due to the martensite variants formed to optimize the accommodation to the tensile stress [4], as further discussed in the following.

Kudoh et al. [10] reported that a possible slip plane in TiNi martensite is $(0\,0\,1)[1\,0\,0]_M$. This slip plane has the largest interplanar distance in the monoclinic B19′

Table 1
Permanent strains of four specimen directions measured from cyclic tensile tests

Orientation to RD	0° (RD)	30°	60°	90° (TD)
Permanent strain (%)	4.9	5.8	3.8	2.7

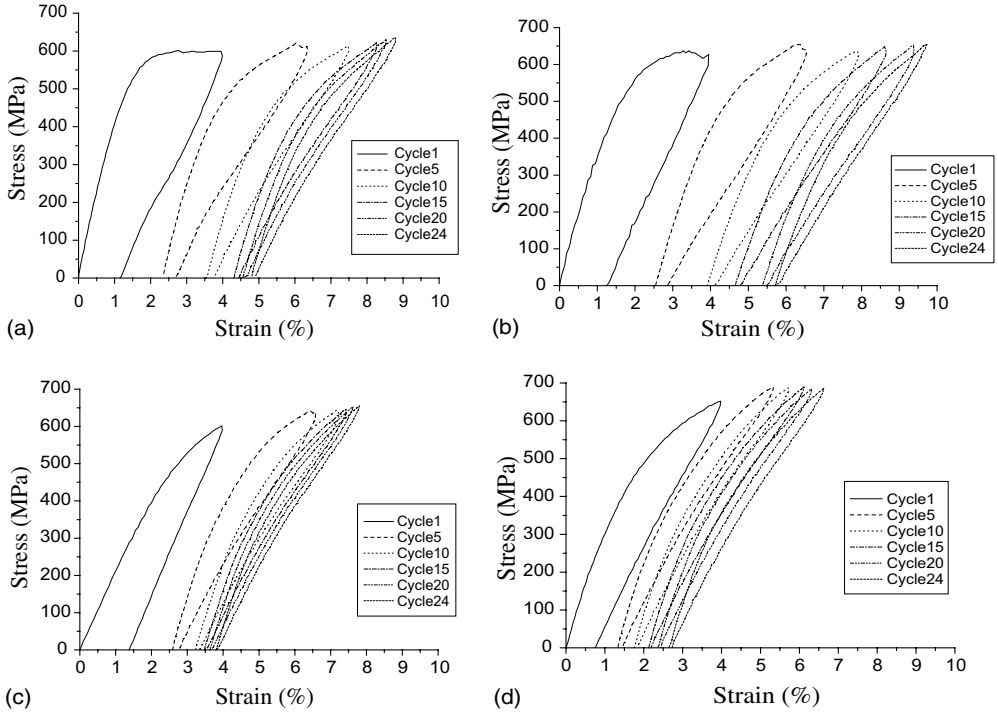

Fig. 3. Stress–strain curves of 24 cyclic tensile tests for various specimen directions: (a) 0°, (b) 30°, (c) 60°, and (d) 90° to rolling direction. The testing temperature is kept at 80 °C.

unit cell and corresponds to the $\{1\,1\,0\}\langle 0\,0\,1\rangle_P$ slip system in the austenite, which is well accepted in the alloys of B2 structure. Mulder et al. [4] calculated the theoretical orientation dependence of Schmid factors for the $(0\,0\,1)[1\,0\,0]_M$ slip system and the four possible martensite textures arising from $(1\,1\,0)[1\,\bar{1}\,0]_P$, the main texture observed in TiNi B2 parent phase. These four possible martensite textures are $(1\,1\,1)[1\,\bar{1}\,\bar{1}]_M$, $(1\,1\,\bar{1})[1\,\bar{1}\,1]_M$, $(0\,1\,0)[0\,0\,1]_M$ and $(0\,0\,1)[0\,1\,0]_M$. Depending on the calculated results [4], the Schmid factors of all four possible martensite textures are almost zero in TD. This leads to the smallest resolved shear stress and the smallest permanent strain appearing in TD, as indicated in Table 1. Also from Table 1, the permanent strain decreases in the order of the specimen's direction in $\theta = 30°$, 0° (RD), 60° and 90° (TD). This sequence fits well with the trend of Schmid factors magnitude for the composition of $(0\,0\,1)[1\,0\,0]_M$ slip system and $(1\,1\,\bar{1})[1\,\bar{1}\,1]_M$ martensite texture [4]. Therefore, in this study, $(1\,1\,\bar{1})[1\,\bar{1}\,1]_M$ is suggested to be the main martensite texture occurring in the B19′ martensite of 50% cold-rolled and 600 °C annealed $Ti_{50}Ni_{50}$ SMA.

3.3. DMA measurement and discussion

In binary TiNi SMAs, there are two kinds of internal friction peaks: a sharp transformation peak due to the martensitic or premartensitic transformation, and a broad relaxation peak occurring at around 200 K [11,12]. From the viewpoint of high damping applications, the latter peak is more important than the former one because, under a constant temperature, the relaxation peak is more stable, whereas the transformation peak decreases rapidly [13].

Fig. 4 shows the relationship between tan delta δ vs. the temperature for specimens in the directions of $\theta = 0°$ (RD), 30°, 60°, 90° (TD). From Fig. 4, the δ values of all specimens in B2 parent phase are almost the same, which means that the damping capacity of TiNi B2 phase is not influenced by the texture. At the same time, all specimens exhibit almost the same sharp transformation peaks at forward and reverse transformation temperatures, which are also not affected by the texture. However, when the temperature reaches 200 K in cooling and 220 K in heating for B19′ martensite shows a relaxation peak for TD and RD specimens, of which the TD specimen has higher peak height. The specimen of $\theta = 60°$ has relatively lower relaxation peak height than those of TD and RD, and the $\theta = 30°$ specimen has no relaxation peak at all.

The appearance of a relaxation peak for TiNi SMAs is usually considered as the twin boundary movement under stress [13]. According to the study of transmission electron microscopy (TEM) in cold-rolled and annealed TiNi sheets [14], most of the twin boundaries in B19′ martensite are found to be $\langle 0\,1\,1\rangle$ type II twinning. From theoretical calculations and TEM observations [15], the easy shear directions of $\langle 0\,1\,1\rangle$ type II twin in the martensite texture $(1\,1\,\bar{1})[1\,\bar{1}\,1]_M$ are almost along the TD, which indicates that the movement of twin boundaries is the easiest in TD. As a result, the specimen in TD has the highest relaxation peak height than in other directions, as observed in Fig. 4. This also provides further evidence that $(1\,1\,\bar{1})[1\,\bar{1}\,1]_M$ is the main martensite texture in 50% cold-rolled and 600 °C annealed $Ti_{50}Ni_{50}$ SMA.

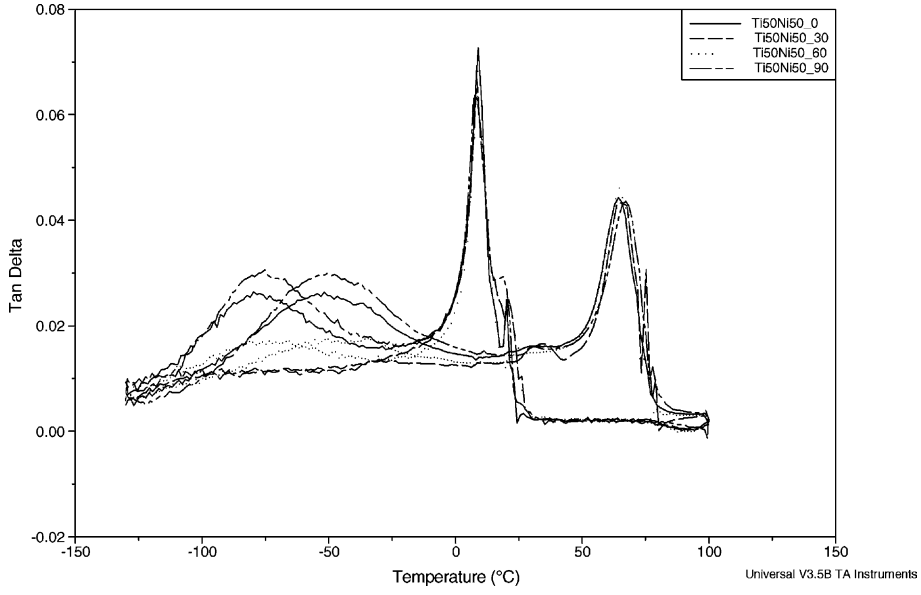

Fig. 4. DMA tan delta δ vs. the temperature curves for specimens along $\theta = 0°$ (RD), 30°, 60°, 90° (TD).

4. Conclusion

Crystallographic textures are investigated from various depths of 50% cold-rolled and 600 °C × 1 h annealed $Ti_{50}Ni_{50}$ sheets by pole figures and ODF. Experimental results show the appearance of two fiber textures. They are $(1\,1\,0)[1\,\bar{1}\,0]_P$ α-fiber II in RD and $(1\,1\,1)[1\,\bar{1}\,0]_P$ γ-fiber in ND with the former having higher orientation density and being regarded as the main texture in the B2 parent phase. The orientation density of γ-fiber decreases from the surface to the 1/2 specimen thickness caused by the shearing effect of the roller's friction. The specimen in TD needs the largest stress than along other directions to reach the same 4% strain in cyclic tensile tests. This is because the Schmid factor in TD is almost zero, which causes the smallest stress-induced-martensite strain in TD. The magnitude of the permanent strain after 24 cycles fits well with the trend of Schimid factors for the composition of $(0\,0\,1)[1\,0\,0]_M$ slip system and $(1\,1\,\bar{1})[1\,\bar{1}\,1]_M$ martensite texture. Therefore, $(1\,1\,\bar{1})[1\,\bar{1}\,1]_M$ is suggested to be the main martensite texture in this study. The height of the relaxation peak becomes the highest in the TD specimen of DMA test, because most of the shear directions of $\langle 0\,1\,1\rangle$ type II twin in $(1\,1\,\bar{1})[1\,\bar{1}\,1]_M$ martensite texture are along TD. This indicates that the movement of twin boundaries is the easiest in TD than along other directions, and also provides further evidence that $(1\,1\,\bar{1})[1\,\bar{1}\,1]_M$ is the main martensite texture.

Acknowledgements

The authors gratefully acknowledge the financial support for this research provided by the National Science Council (NSC), Taiwan, Republic of China, under grants no. NSC91-2216-E002-035.

References

[1] Wayman CM, During TW. In: During TW, Melton KN, Stöckel D, Wayman CM, editors. Engineering aspects of shape memory alloys. London: Butterworth-Heinemam Press; 1990. p. 3–20.
[2] Eucken S, Hirsch J. Mater Sci Forum 1990;56–58:487.
[3] Lin HC, Wu SK, Chou TS, Kao HP. Acta Metall Mater 1991;39:2069.
[4] Mulder JH, Thoma PE, Beyer J. Z Metallkd 1993;84:501.
[5] Inoue H, Miwa N, Inakazu N. Acta Mater 1996;44:4825.
[6] Shu YC, Bhattacharya K. Acta Mater 1998;46:5457.
[7] Miyazaki S, No VH, Kitamura K, Khantachawana A, Hosoda H. Int J Plast 2000;16:1135.
[8] Bunge HJ. Texture analysis in materials science. London: Butterworths; 1982. p. 25–29.
[9] Raabe D, Lücke K. Mater Sci Forum 1994;157–162:597.
[10] Kudoh Y, Tokonami M, Miyazaki S, Otska K. Acta Metall 1985;33:2049.
[11] Mercier O, Melton KN, Preville Y. Acta Metall 1979;27:1467.
[12] Wu SK, Lin HC, Chou TS. Acta Metall 1990;27:1467.
[13] Yoshida I, Monma D, Iino K, Otsuka K, Asai M, Tsuzuki H. J Alloys Compd 2003;355:79.
[14] Nashida M, Ohgi H, Itai I, Chiba A, Yamauchi K. Acta Metall Mater 1995;43:1219.
[15] Liu Y, Xie ZL, Humbeek JV, Delaey L. Acta Mater 1999;47:645.